machines

MDPI

Article

Milling-Force Prediction Model for 304 Stainless Steel Considering Tool Wear

Changxu Wang [1], Yan Li [1,*], Feng Gao [1], Kejun Wu [1], Kan Yin [1], Peng He [1] and Yunjiao Xu [2]

[1] School of Mechanical and Precision Instrument Engineering, Xi'an University of Technology, Xi'an 710048, China; 15315216859@163.com (C.W.); gf2713@xaut.edu.cn (F.G.); bestafter@163.com (K.W.); 15934486412@163.com (K.Y.); hp19991624011@163.com (P.H.)

[2] School of Machinery and Automation, Weifang University, Weifang 262799, China; xyj18053647607@163.com

* Correspondence: liyangf@xaut.edu.cn

Abstract: The high-performance alloy, 304 stainless steel, is widely used in various industries. However, its material properties lead to severe tool wear during milling processes, significantly increasing milling force and adversely impacting machining quality and efficiency. Consequently, an accurate milling-force model is crucial for guiding the formulation and optimization of machining parameters. This paper presents a milling-force prediction model for 304 stainless steel that incorporates the effect of tool wear, based on the mechanistic modeling approach. Side-milling experiments on 304 stainless steel were conducted to analyze the relationship between milling force and tool wear, identify the model coefficients, and validate the prediction accuracy of the milling-force model. The results demonstrate that the model accurately predicts the milling forces of worn tools while side milling 304 stainless steel under various machining parameters and tool wear conditions.

Keywords: 304 stainless steel; tool wear; model coefficient identification; milling-force prediction

check for updates

Academic Editors: Feiyan Guo and Zhengping Chang

Received: 26 December 2024
Revised: 17 January 2025
Accepted: 18 January 2025
Published: 20 January 2025

Citation: Wang, C.; Li, Y.; Gao, F.; Wu, K.; Yin, K.; He, P.; Xu, Y. Milling-Force Prediction Model for 304 Stainless Steel Considering Tool Wear. *Machines* **2025**, *13*, 72. https://doi.org/10.3390/machines13010072

Copyright: © 2025 by the authors. Licensee MDPI, Basel, Switzerland. This article is an open access article distributed under the terms and conditions of the Creative Commons Attribution (CC BY) license (https://creativecommons.org/licenses/by/4.0/).

1. Introduction

Due to excellent mechanistic strength, heat resistance, ductility, and corrosion resistance [1,2], components made of 304 stainless steel are durable, reliable, and aesthetically appealing [3]. Consequently, it is widely utilized in the medical, chemical, energy, defense, and aerospace industries [4]. Because of its high mechanistic strength and tendency toward hardening, 304 stainless steel requires a significant cutting force during machining. Additionally, its low thermal conductivity causes heat to accumulate in the cutting zone, increasing the temperature at the cutting edge. The high affinity and ductility of 304 stainless steel further lead to chips adhering to the tool surface, forming a built-up edge (BUE), which contributes to rapid tool wear [5,6]. As the tool wears, the ploughing force on the flank face increases, significantly increasing cutting force [7]. When machining a workpiece with relatively low stiffness (especially thin-walled components), excessive cutting forces can deform the workpiece, resulting in machining errors [8]. An increase in cutting force can affect the elastic and plastic deformation of the workpiece surface as well as the cutting temperature, thereby influencing the surface machining quality [9]. An increase in cutting force results in higher cutting power, thereby contributing to an increase in the energy consumption of the machine tool [10]. In summary, the significant increase in cutting force caused by tool wear during actual machining can adversely affect both machining quality and efficiency. Bhushan et al. [11] calculated milling forces under various machining parameters using the developed cutting-force model and optimized parameters

with milling force as the objective. Liu et al. [12] processed the milling-force signals using the cutting-force model that considers tool wear, enabling the monitoring of tool wear. Du et al. [13] calculated the milling forces under different machining parameters using the milling-force model, and by considering the effect of milling forces on tool deflection, they analyzed the tool's motion trajectory to predict the surface roughness of the machined part. Therefore, it is evident that the milling-force model can be applied to optimize machining parameters, monitor tool wear, and predict surface quality. To improve machining quality and efficiency and mitigate the adverse effects caused by the significant increase in cutting force due to tool wear, establishing an accurate and easily applicable milling-force model that considers tool wear is essential.

At present, there are five main models of cutting force: the empirical model, analytical model, mechanistic model, finite element model, and data-driven model. The empirical model relies on data from cutting-force tests or actual production and uses statistical methods to establish the relationship between cutting force and machining parameters [14]. The analytical model employs orthogonal or oblique cutting theory to analyze the cutting process from both geometric and mechanistic perspectives and determine the cutting force, which was founded by Merchant's research [15,16]. The mechanistic model proposed by Altintas assumes the cutting force as the product of the area of cutting zone and the cutting-force coefficient, based on the analysis of cutting conditions, in which a cutting experiment is conducted to identify the cutting-force coefficients [17]. Commercial FEA (finite element analysis) software is used to visually simulate cutting forces under various cutting conditions [18]. The data-driven model uses neural networks or deep learning to analyze large datasets and establish the mapping relationship between cutting force and working conditions through an evolution learning mechanism [19].

Compared to the other four models, the mechanistic model of cutting force emphasizes the engagement relationship between the tool and workpiece during the cutting process, using numerical methods to efficiently handle complex cutting conditions. As a result, the mechanistic model is widely used to establish milling-force models that consider tool wear. Zhao et al. [20] replaced the actual wear with the wear width of the flank face and introduced a variable attenuation coefficient in the stress distribution function to develop a milling-force prediction model for worn ball-end tools considering the effect of rebound. Wojciechowski et al. [21] considered the effects of friction, rubbing, and ploughing mechanisms between the workpiece and tool flank face during machining and investigated the cutting forces in the ball-end milling of inclined surfaces. Wang et al. [22] developed a milling-force model for an asymmetric micro milling cutter, including the effect of tool wear on instantaneous undeformed chip thickness, shear/ploughing force and friction in the wear zone of the flank face. Gao et al. [23] derived an instantaneous undeformed chip-thickness model and proposed a milling-force prediction model for worn micro-end mills by accounting for the effects of flute radius and flank wear on tool runout. Liu et al. [24] developed a micro-milling-force model, combining the influences of tool runout, cutting-edge radius and tool wear by integrally calculating the instantaneous undeformed chip thickness, shear-force and ploughing-force coefficients. Wojciechowski et al. [25] considered the geometric errors, tool deflections, minimum uncut chip thickness, and chip-thickness accumulation in the machining system, and using a combined numerical-analytical approach, they evaluated the minimum uncut chip thickness, ploughing, and shearing forces, further developing a milling-force model for the micro-milling of AISI 1045 steel. Hou et al. [26] decomposed the cutting force of a worn tool into shear force and friction forces, explaining the distribution of friction stress on the flank face to build a milling-force model for a worn tool, with the model coefficients identified experimentally. Huang et al. [27], considering the complexity arising from tool geometry, applied a genetic algorithm to determine the

coefficients of the cutting-force model, thereby establishing a cutting-force model for worn CBN tools to turn hardened 52100 bearing steel. Chinchanikar et al. [28] extended the Waldorf's orthogonal cutting-force modeling method into a three-dimensional model. By using an equivalent cutting-edge geometry to determine the shear angle, chip flow angle, and other model parameters, a regression analysis method was employed to establish a cutting-force model for turning quenched AISI 4340 steel with a worn tool. Patel et al. [29] conducted the full factorial turning experiments of hardened AISI D2 steel and extended an empirical model of cutting force based on Waldorf's theory considering tool wear. Toubhans et al. [30] analyzed the engagement area between the tool and the workpiece, developing a time-varying cutting-force model for tool wear in the turning of Inconel 718, considering the effect of cutting speed and feed rate on tool wear, and adding an additional time-dependent term to the cutting-force coefficient.

Based on the above research, cutting-force modeling considering tool wear has primarily focused on micro-milling and turning processes. However, in practical manufacturing, side milling serves as the primary machining method for most metals and some difficult-to-machine materials. Since 304 stainless steel is widely used and prone to tool wear during machining, this paper establishes a milling-force model considering tool wear, based on side-milling experiments conducted with 304 stainless steel. It also visually demonstrates the tool wear process and the variation of milling forces with tool wear. To improve the model's precision, this paper incorporates the effect of tool wear on the actual tool radius. A method to calculate method for the worn tool's actual radius has been derived and applied in the calculation of tool entry/exit angle and the instantaneous undeformed chip thickness. While most studies adopt Altintas' [17] quick identification method for milling-force coefficients, which necessitates slot milling conditions, it is important to note that slot milling can significantly affect tool life, especially when processing difficult-to-cut metals. Therefore, this study proposes a milling-force coefficient identification method, based on average milling forces, that is suitable for side-milling conditions, in conjunction with the established milling-force model. The remaining sections of this paper are organized as follows: In Section 2, the worn end mill is discretized into cutting-edge elements for cutting-force analysis. Based on the engagement relationship examined between tool and workpiece, and an instantaneous milling-force mechanistic model for the worn tool is derived. In Section 3, a method for identifying milling-force model coefficients using average milling forces is proposed. Side-milling experiments on 304 stainless steel were conducted to identify the model coefficients and validate the accuracy of the model. In Section 4, the study's findings, the model's limitations, and its potential industrial applications are discussed. Finally, Section 5 summarizes the conclusions.

2. Mechanistic Modeling of Milling Forces for Worn Tools

2.1. Geometrical Discretization Method for the Cutting Edge

Figure 1 illustrates the geometric relationship during the side-milling process using a four-flute end mill. A right-handed Cartesian coordinate system (O-XYZ) is established, positioning the origin O at the bottom center of the end mill. The Z axis aligns with the tool's axis, the Y axis extends along the tool's feed direction, and the X axis is perpendicular to the YZ plane. This coordinate system aligns with the machine tool's coordinate system.

The end mill is discretized into multiple cutting-edge elements along the Z axis. As an example, consider the cutting-edge element P shown in Figure 1. The position of any arbitrary cutting-edge element during the milling process is determined by the tool–workpiece engagement angle θ, which is calculated as follows:

$$\theta = \left(\varphi + \frac{2\pi}{N}(i-1) + \frac{z\tan\beta}{R_{ac}}\right) \mathrm{mod} 2\pi \quad (1)$$

where N is the total number of cutting edges, i is the index of the cutting edges, z is the height of the cutting-edge element from the bottom of the tool edge, β is the helix angle of the tool, R_{ac} is the actual radius of the tool, mod represents the modulus operation, and φ is the rotation angle of the end mill. The rotation angle φ can be calculated as follows:

$$\varphi = \omega t \tag{2}$$

where ω is the spindle speed and t is the milling time.

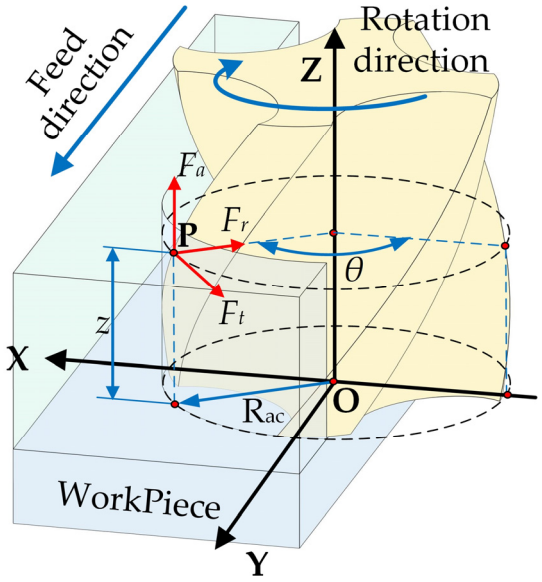


Figure 1. Geometric relationship during side-milling process of an end mill.

2.2. Force Analysis of Cutting-Edge Elements for Worn Tools

During the milling process, the cutting-edge elements experience tangential force dF_t, radial force dF_r, and axial force dF_a (where the tangential t, radial r, and axial a directions are defined as follows: the tangential direction t is along the direction of the cutting-edge velocity, the radial direction r points toward the tool axis along the tool radius, and the axial direction a is perpendicular to both the tangential and radial directions, oriented vertically along the tool axis).

When the cutting edge is sharp or exhibits no significant wear, the ploughing effect on the flank face is very weak, and there is almost no extrusion or friction between the flank face and the workpiece. This assumes that the tool is only subjected to the shearing force generated by the rake face [20,26], including the tangential shear force dF_{tc}, radial shear force dF_{rc}, and axial shear force dF_{ac}, as shown in Figure 2.

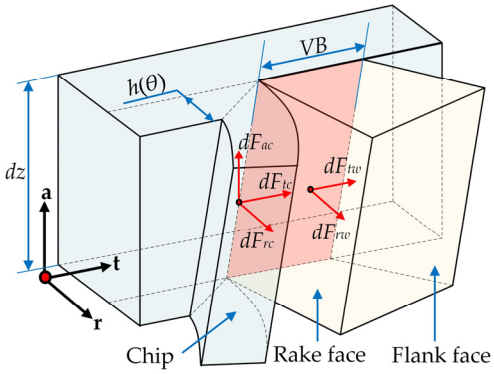


Figure 2. Forces on the cutting-edge element of a worn end mill.

When a significant wear area appears on the flank face (highlighted in red in Figure 2), extrusion and friction occur between the worn tool's flank face and the machined surface, resulting in a ploughing effect. Since the wear on the flank face does not generate an axial ploughing force [31], the ploughing force is decomposed into tangential contact force dF_{tw} and radial contact force dF_{rw}.

Based on the geometric relationship, the tangential force dF_t, radial force dF_r, and axial force dF_a are expressed as follows:

$$\begin{cases} dF_t &= dF_{tc} + dF_{tw} \\ dF_r &= dF_{rc} + dF_{rw} \\ dF_a &= dF_{ac} \end{cases} \tag{3}$$

Based on the mechanistic cutting-force model established by Altintas [17], the further derivation of Equation (3) leads to an expression for the cutting force on the cutting-edge element at any tool–workpiece engagement angle θ as follows:

$$\begin{cases} dF_t(\theta) &= K_{tc}h(\theta)dz + K_{tw}(VB)dz \\ dF_r(\theta) &= K_{rc}h(\theta)dz + K_{rw}(VB)dz \\ dF_a(\theta) &= K_{ac}(VB)h(\theta)dz \end{cases} \tag{4}$$

where $h(\theta)$ is the thickness of the instantaneous undeformed chip, VB is the tool flank-wear width, and K_{tc}, K_{rc} and $K_{ac}(VB)$ represent the tangential, radial and axial shear-force coefficients, respectively. Meanwhile, $K_{tw}(VB)$, and $K_{rw}(VB)$ represent the tangential and radial contact-force coefficients. $K_{ac}(VB)$, $K_{tw}(VB)$, and $K_{rw}(VB)$ are expressed as functions of VB. dz represents the height of the cutting-edge element, and the corresponding calculation equation is given as follows:

$$dz = \frac{R_{ac}d\theta}{\tan\beta} \tag{5}$$

2.3. Analysis of Tool–Workpiece Engagement Relationship

The instantaneous milling force of the end mill is the sum of the cutting forces from all cutting-edge elements. Since not all the cutting-edge elements engage in the milling process simultaneously, it is essential to calculate the tool entry and exit angle of the end mill to determine the range of the milling area. As the flank wear progresses, the actual radius of the tool decreases, which leads to changes in the tool entry angle, tool exit angle and instantaneous undeformed chip thickness, which in turn affect the milling force.

2.3.1. Calculation of Actual Radius for Worn End Mills

In order to analyze the variation of the actual radius of the end mill during the tool wear process, an orthogonal cutting-edge coordinate system $X_eO_eY_e$ is established at the bottom edge of the tool, as shown in Figure 3. The origin O_e is positioned at the cutting edge, with the Y_e axis directed from the bottom cutting edge to the top cutting edge. The X_e axis is perpendicular to the Y_e axis and tangent to the cutting-edge arc. The worn area of the tool is represented by segment OeAB, where segment O_eA corresponds to the rake face and segment O_eB corresponds to the flank face. According to the geometric relationship, as the flank face wears, the actual radius of the tool decreases. The calculation equation is as follows:

$$R_{ac} = \sqrt{\left(\frac{VB \times \sin\gamma}{\cos(\alpha+\gamma)}\right)^2 + R^2 - \frac{2 \times VB \times R \times \cos\alpha \times \sin\gamma}{\cos(\alpha+\gamma)}} \tag{6}$$

where R is the radius of the sharp end mill, and α and γ represent the tool's rake angle and flank angle of the tool, respectively.

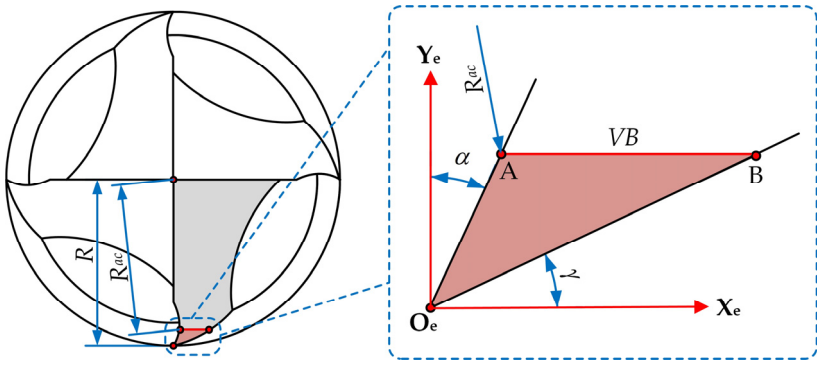


Figure 3. Actual radius of the worn end mill.

2.3.2. Calculation of Tool Entry and Exit Angle

In the side milling of 304 stainless steel, a small cutting width is typically used for climb milling. Figure 4 shows the geometric relationship of the tool–workpiece engagement during climb milling with a cutting width $a_e < R_{ac}$. The angle at which the cutting edge first engages the workpiece is defined as the tool entry angle θ_{en}. At this point, the instantaneous undeformed chip thickness starts from zero and increases. It reaches its maximum value at the transition angle θ_{tr} and then gradually decreases until it becomes zero at the exit angle θ_{ex}, when the tool exits the workpiece. The geometric relationship between the tool entry angle, transition angle and tool exit angle can be expressed as follows:

$$\begin{cases} \theta_{en} = \pi - \arccos\left(1 - \frac{R_{ac}}{a_e}\right) \\ \theta_{tr} = \pi - \arctan\left(\frac{\sqrt{{R_{ac}}^2 - (R_{ac} - a_e)^2} - f_z}{R_{ac} - a_e}\right) \\ \theta_{ex} = \pi + \arcsin\left(\frac{f_z}{2 \times R_{ac}}\right) \end{cases} \tag{7}$$

where f_z is the feed per tooth.

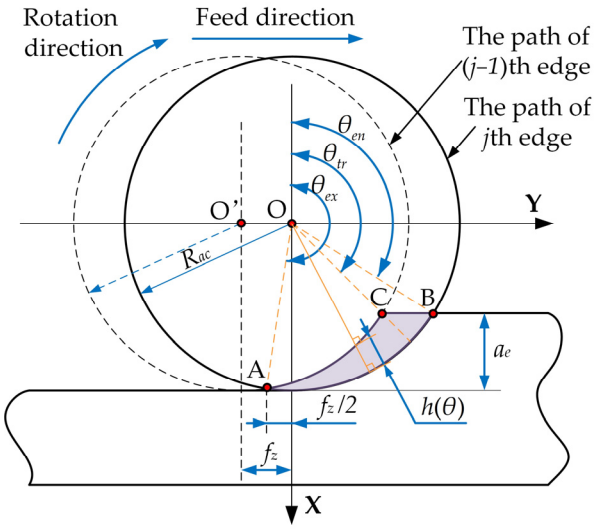


Figure 4. Geometric relationship of the end mill during climb milling.

2.3.3. Calculation of Instantaneous Undeformed Chip Thickness

In the milling process, the relative motion between the end mill and the workpiece can be decomposed into linear motion and rotation. Therefore, the motion of the cutting

edge is described by a complex cycloidal motion. Due to the small feed per tooth and the high rotational speed of the end mill, the actual trajectory of the cutting edge can be assumed to be a circular arc [32]. As shown in Figure 4, AC represents the surface formed by the previous cutting edge removing the workpiece material, while AB represents the surface formed by the current cutting edge. The radial distance between two adjacent surfaces is referred to as the instantaneous undeformed chip thickness. Based on the geometric relationship shown in Figure 4, the instantaneous undeformed chip thickness can be derived as follows:

$$h(\theta) = \begin{cases} R_{ac} - \frac{R_{ac} - a_e}{\cos(\pi - \theta)} & \theta_{en} \le \theta \le \theta_{tr} \\ R_{ac} + f_z \sin\theta - \sqrt{{R_{ac}}^2 - {f_z}^2 \cos^2\theta} & \theta_{tr} \le \theta \le \theta_{ex} \end{cases} \tag{8}$$

2.4. Calculation of Instantaneous Milling Force

Based on the geometric relationship during side milling of the end mill shown in Figure 1, the tangential force dF_t, radial force dF_r and axial force dF_a acting on the cutting-edge element at the tool–workpiece engagement angle θ are transformed into the O-XYZ coordinate system. The calculation equation is as follows:

$$\begin{bmatrix} dF_x(\theta) \\ dF_y(\theta) \\ dF_z(\theta) \end{bmatrix} = J(\theta)T(\theta) \begin{bmatrix} dF_t(\theta) \\ dF_r(\theta) \\ dF_a(\theta) \end{bmatrix} \tag{9}$$

where $J(\theta)$ is a step function used to determine whether the cutting-edge element participates in the milling process, defined as

$$J(\theta) = \begin{cases} 1 & if\ \theta_{en} \le \theta \le \theta_{ex} \\ 0 & otherwise \end{cases} \tag{10}$$

$T(\theta)$ is the coordinate transformation matrix, defined as

$$T(\theta) = \begin{bmatrix} -\sin\theta & \cos\theta & 0 \\ -\cos\theta & -\sin\theta & 0 \\ 0 & 0 & 1 \end{bmatrix} \tag{11}$$

In the milling process, based on the tool–workpiece engagement relationship at different moments, the forces acting on each cutting-edge element within the milling range of each cutting edge are integrated. By summing the forces acting on each cutting edge, the instantaneous milling force acting on the end mill at the rotational angle φ is obtained as follows:

$$\begin{aligned} \begin{bmatrix} F_x \\ F_y \\ F_z \end{bmatrix}_{(\varphi)} = & \begin{bmatrix} \sum_{i=1}^{N} \int_{\theta_{en}}^{\theta_{ex}} -\sin\theta J(\theta)h(\theta)dz & \sum_{i=1}^{N} \int_{\theta_{en}}^{\theta_{ex}} \cos\theta J(\theta)h(\theta)dz & 0 \\ \sum_{i=1}^{N} \int_{\theta_{en}}^{\theta_{ex}} -\cos\theta J(\theta)h(\theta)dz & \sum_{i=1}^{N} \int_{\theta_{en}}^{\theta_{ex}} -\sin\theta J(\theta)h(\theta)dz & 0 \\ 0 & 0 & \sum_{i=1}^{N} \int_{\theta_{esn}}^{\theta_{ex}} J(\theta)h(\theta)dz \end{bmatrix} \begin{bmatrix} K_{tc} \\ K_{rc} \\ K_{ac}(VB) \end{bmatrix} \\ & + \begin{bmatrix} \sum_{i=1}^{N} \int_{\theta_{en}}^{\theta_{ex}} -\sin\theta J(\theta)dz & \sum_{i=1}^{N} \int_{\theta_{ex}}^{\theta_{ex}} \cos\theta J(\theta)dz & 0 \\ \sum_{i=1}^{N} \int_{\theta_{en}}^{\theta_{ex}} -\cos\theta J(\theta)dz & \sum_{i=1}^{N} \int_{\theta_{ex}}^{\theta_{ex}} -\sin\theta J(\theta)hdz & 0 \\ 0 & 0 & \sum_{i=1}^{N} \int_{\theta_{en}}^{\theta_{ex}} J(\theta)h(\theta)dz \end{bmatrix} \begin{bmatrix} K_{tw}(VB) \\ K_{rw}(VB) \\ 0 \end{bmatrix} \end{aligned} \tag{12}$$

3. Milling Experiment and Analysis

Side-milling experiments on 304 stainless steel were conducted on a three-axis machining center, using climb milling as the cutting method. The tool employed was a Heye and Sumitomo high-speed steel end mill, with the tool geometric parameters detailed in Table 1. The experimental setup and equipment layout are shown in Figure 5, with the models of the equipment listed in Table 2.

Table 1. Geometric parameters of the end mill.

Diameter (mm)	Number of Edges	Helix Angle (°)	Rake Angle (°)	Flank Angle (°)
8	4	30	12	12

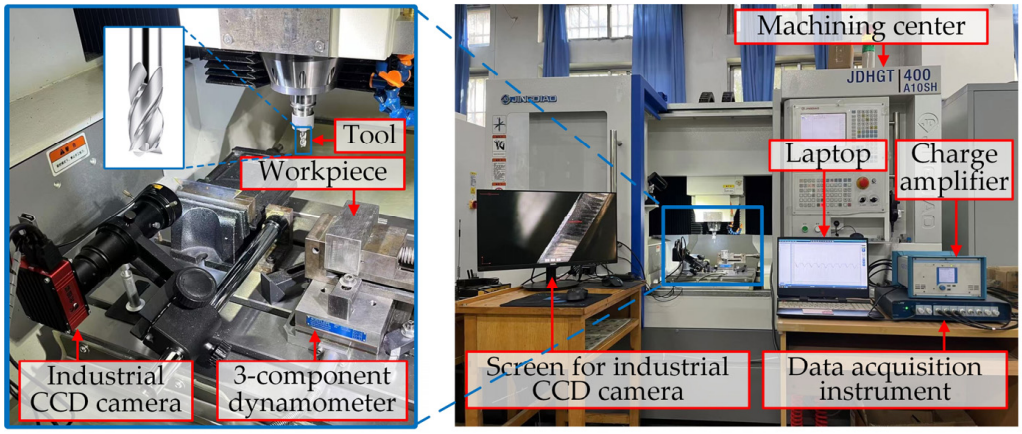


Figure 5. Experimental setup and equipment layout.

Table 2. Experimental equipment and their models.

Equipment	Model
Machining center (Beijing Jingdiao Co., Ltd., Beijing, China)	JDHGT400A10SH
Three-component dynamometer (Kistler Co., Ltd, Winterthur, Switzerland)	Kistler 9257B
Charge amplifier (Kistler Co., Ltd., Winterthur, Switzerland)	Kistler 5070
Data acquisition instrument (Econ Co., Ltd., Hangzhou, China)	Yiheng MI7008
Industrial CCD camera (BeiYinHu Optics (Shenzhen) Co., Ltd., Shenzhen, China)	RZSP-2KCH

Measurement of milling forces: Milling-force signals were measured using a Kistler 9257B three-component dynamometer, processed by a Kistler 5070 charge amplifier, and saved to a laptop via a Yiheng MI7008 data acquisition instrument with a sampling frequency of 12 kHz.

Measurement of tool flank-wear widths (*VB*): The *VB* value was obtained through image processing the tool flank wear, captured by the RZSP-2KCH industrial CCD camera, in accordance with the ISO 8688-2: 1989 [33] standard. To minimize human error during the measurement process, each measurement was taken at a fixed position, with five measurements performed per blade, and the results were averaged.

3.1. Identification of Milling-Force Model Coefficients

3.1.1. Coefficient-Identification Method

Based on the calculation method for the average milling force of a single cutting edge proposed in reference [17], and combined with Equation (12), an equation for calculating the average cutting force of the entire tool over any given cycle can be further derived as

$$\begin{bmatrix} \overline{F_x} \\ \overline{F_y} \\ \overline{F_z} \end{bmatrix} = \frac{1}{\varphi_{fi} - \varphi_{st}} \int_{\varphi_{st}}^{\varphi_{fi}} \begin{bmatrix} F_x \\ F_y \\ F_z \end{bmatrix}_{(\varphi)} d\varphi \tag{13}$$

where φ_{st} is the spindle rotation angle at the start of milling and φ_{fi} is the spindle rotation angle at the end of milling.

It has been assumed that only the shearing effect of the rake face exists when the tool is sharp. Combined with Equations (12) and (13), it can be inferred that the tangential shear-force coefficient K_{tc}, the radial shear-force coefficient K_{rc} and the axial shear-force coefficient $K_{ac}(VB)$ when the tool is unworn can be identified by the average milling force of the sharp end mill. The equation is as follows:

$$\begin{bmatrix} K_{tc} \\ K_{rc} \\ K_{ac}(VB) \end{bmatrix} = \begin{bmatrix} \sum_{i=1}^{N} \int_{\varphi_{st}}^{\varphi_{fi}} \int_{\theta_{en}}^{\theta_{ex}} -\sin\theta J(\theta) h(\theta) dz d\varphi & \sum_{i=1}^{N} \int_{\varphi_{st}}^{\varphi_{fi}} \int_{\theta_{en}}^{\theta_{ex}} \cos\theta J(\theta) h(\theta) dz d\varphi & 0 \\ \sum_{i=1}^{N} \int_{\varphi_{st}}^{\varphi_{fi}} \int_{\theta_{en}}^{\theta_{ex}} -\cos\theta J(\theta) h(\theta) dz d\varphi & \sum_{i=1}^{N} \int_{\varphi_{st}}^{\varphi_{fi}} \int_{\theta_{en}}^{\theta_{ex}} -\sin\theta J(\theta) h(\theta) dz d\varphi & 0 \\ 0 & 0 & \sum_{i=1}^{N} \int_{\varphi_{st}}^{\varphi_{fi}} \int_{\theta_{en}}^{\theta_{ex}} J(\theta) h(\theta) dz d\varphi \end{bmatrix}^{-1} \begin{bmatrix} \overline{F_x} \\ \overline{F_y} \\ \overline{F_z} \end{bmatrix} \tag{14}$$

Since only shear force acts in the axial direction [31], the axial shear-force coefficient $K_{ac}(VB)$ for the worn tool is also identified using Equation (14).

Tool wear leads to friction and extrusion between the tool flank face and the workpiece, generating ploughing force. The ploughing-force coefficients include the tangential contact-force coefficient $K_{tw}(VB)$ and the radial contact-force coefficient $K_{rw}(VB)$. The ploughing-force coefficients at different tool flank-wear widths are identified by the difference between the average cutting forces in the X and Y directions at the current tool flank-wear width and the sharp tool condition. By combining Equations (12) and (13), the ploughing-force coefficients can be identified by the following equation:

$$\begin{bmatrix} K_{tw}(VB) \\ K_{rw}(VB) \end{bmatrix} = \begin{bmatrix} \sum_{i=1}^{N} \int_{\varphi_{st}}^{\varphi_{fi}} \int_{\theta_{en}}^{\theta_{ex}} -\sin\theta J(\theta) dz d\varphi & \sum_{i=1}^{N} \int_{\varphi_{st}}^{\varphi_{fi}} \int_{\theta_{ex}}^{\theta_{en}} \cos\theta J(\theta) dz d\varphi \\ \sum_{i=1}^{N} \int_{\varphi_{st}}^{\varphi_{fi}} \int_{\theta_{en}}^{\theta_{ex}} -\cos\theta J(\theta) dz d\varphi & \sum_{i=1}^{N} \int_{\varphi_{st}}^{\varphi_{fi}} \int_{\theta_{ex}}^{\theta_{en}} -\sin\theta J(\theta) dz d\varphi \end{bmatrix}^{-1} \times \left[\begin{bmatrix} \overline{F_x}(VB) \\ \overline{F_y}(VB) \end{bmatrix} - \begin{bmatrix} \overline{F_{xs}} \\ \overline{F_{ys}} \end{bmatrix} \right] \tag{15}$$

where $\overline{F_x}(VB)$, $\overline{F_y}(VB)$ represent the average milling forces in the X and Y directions at the current tool flank-wear width, $\overline{F_{xs}}$, $\overline{F_{ys}}$ represent the average milling forces in the X and Y directions when the tool is sharp.

3.1.2. Experimental Identification Results

A side-milling experiment on 304 stainless steel was conducted to identify the coefficients K_{tc}, K_{ac}, $K_{ac}(VB)$, $K_{tw}(VB)$ and $K_{rw}(VB)$. The experimental parameters are shown in Table 3.

Table 3. Milling-force model coefficient-identification experiment.

Spindle Speed S (r/min)	Feed per Tooth f_z (mm/tooth)	Axial Depth a_p (mm)	Radial Depth a_e (mm)
750	0.04	3	0.5

The end mill performs climb milling along the Y-axis. The length of the workpiece in the Y direction is 100 mm. A milling cycle is defined as the tool's feeding along the Y-axis by 100 mm. A tool-rotation cycle is defined as a full 360° rotation of the tool. The flank wear is measured and the milling forces are recorded every time the flank wear increases by approximately 0.05 mm. The tool flank-wear widths and the corresponding milling forces are shown in Figure 6.

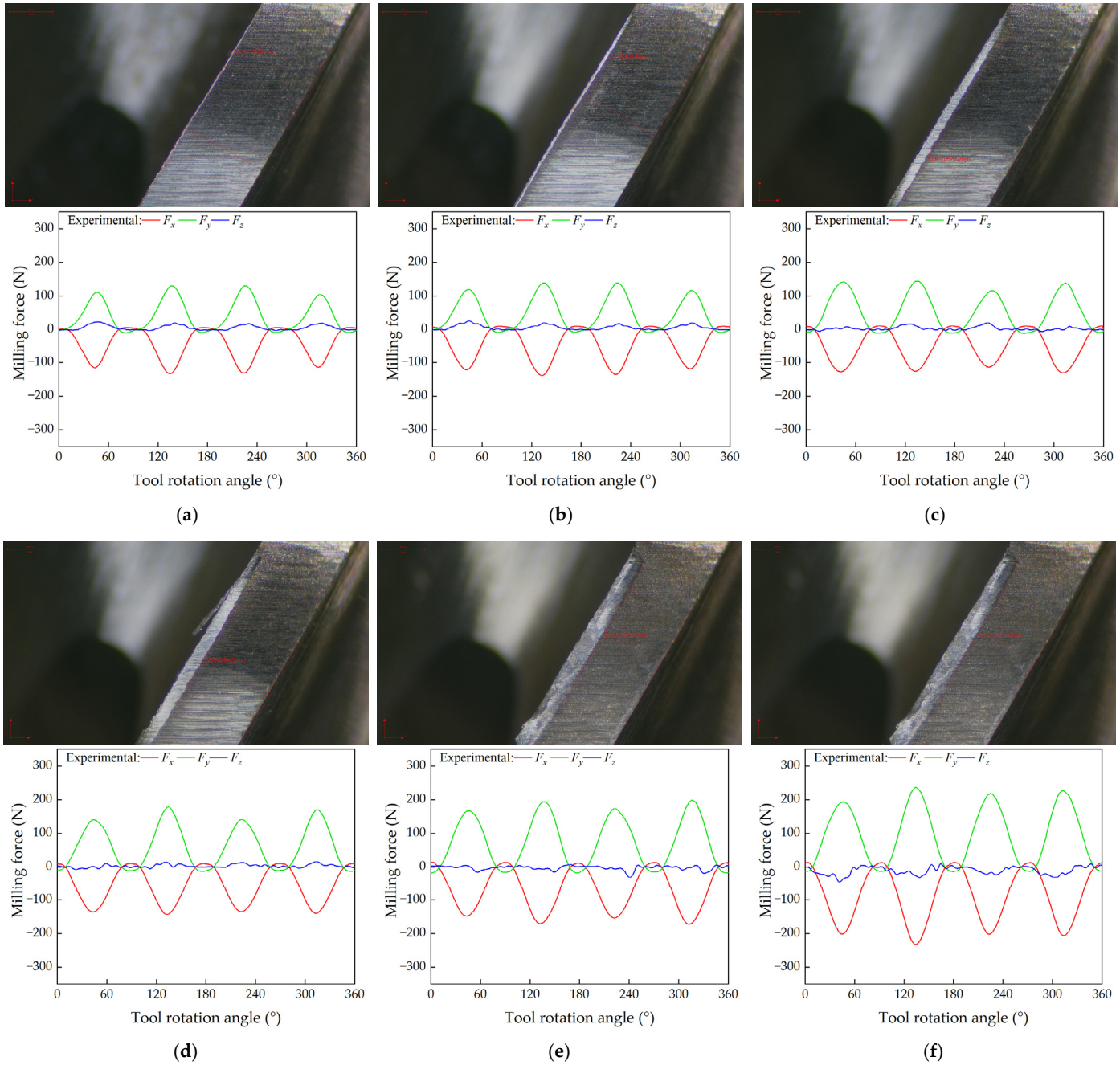
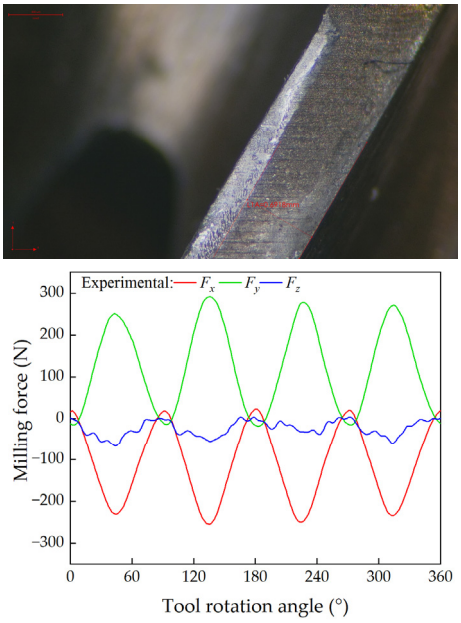


Figure 6. *Cont.*



(**g**)

Figure 6. Tool flank-wear widths with corresponding milling forces: (**a**) VB = 0 mm; (**b**) VB = 0.0521 mm; (**c**) VB = 0.1038 mm; (**d**) VB = 0.1508 mm; (**e**) VB = 0.2013 mm; (**f**) VB = 0.253 mm; (**g**) VB = 0.3022 mm.

Equations (14) and (15) were used to identify the milling-force model coefficients. To minimize errors in the identification process and reduce randomness, milling forces were selected from five randomly chosen tool-rotation cycles (with each cycle being random and non-continuous) within a milling cycle. These milling-force data will be used to calculate the average milling force, which is used for the identification of the model coefficients. The identification results of $K_{ac}(VB)$, $K_{tw}(VB)$, and $K_{rw}(VB)$ under varying tool flank-wear widths are shown in Figure 7. These coefficients were then fitted as functions of the VB value. A summary of the identification results of all the milling-force model coefficients is provided in Table 4.

Table 4. Coefficients of the milling-force model.

Coefficients of Shear Force	
K_{tc} (N/mm^2)	5532.29
K_{rc} (N/mm^2)	2850.51
$K_{ac}(VB)$ (N/mm^2)	$-135760.81 \times VB^3 + 10268.67 \times VB^2 - 621.92 \times VB + 549.1$
Coefficients of Ploughing Force	
$K_{tw}(VB)$ (N/mm)	$3320.59 \times VB^3 - 339.45 \times VB^2 + 127.86 \times VB - 0.22$
$K_{rw}(VB)$ (N/mm)	$835.05 \times VB^3 + 238.77 \times VB^2 - 3.36 \times VB + 0.59$

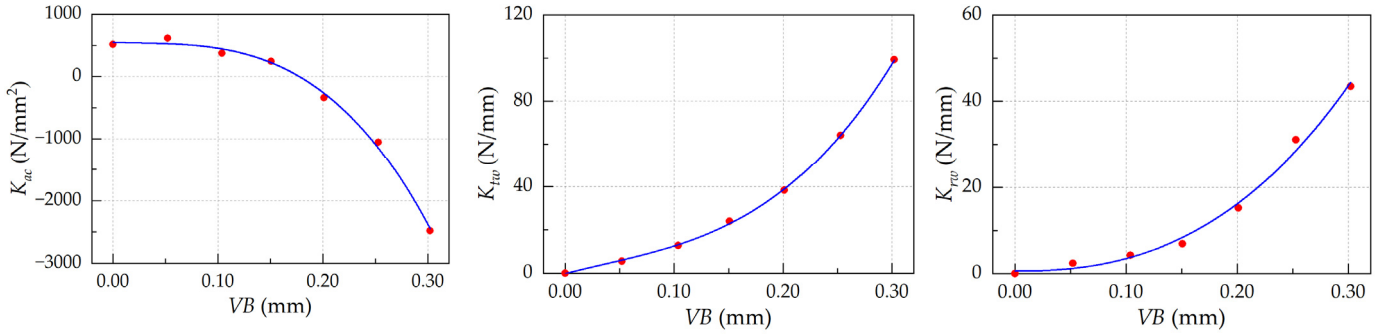


Figure 7. The variation of $K_{ac}(VB)$, $K_{tw}(VB)$ and, $K_{rw}(VB)$ with VB.

3.2. Validation of the Milling-Force Model

Two end mills were employed to conduct the following six experiments to validate the accuracy of the milling-force prediction model for worn end mills. The experimental parameters are shown in Table 5.

Table 5. Milling-force model validation experiments.

Test.	Spindle Speed S (r/min)	Feed per Tooth f_z (mm/tooth)	Axial Depth a_p (mm)	Radial Depth a_e (mm)	Tool Flank-Wear Width VB (mm)
1	830	0.05	3.5	0.6	0
2					0.1098
3					0.2109
4	900	0.03	4	0.7	0
5					0.1185
6					0.2003

Figure 8 shows the flank-wear images for each experiment, along with the comparison curves of the corresponding experimental milling forces and the predicted milling forces.

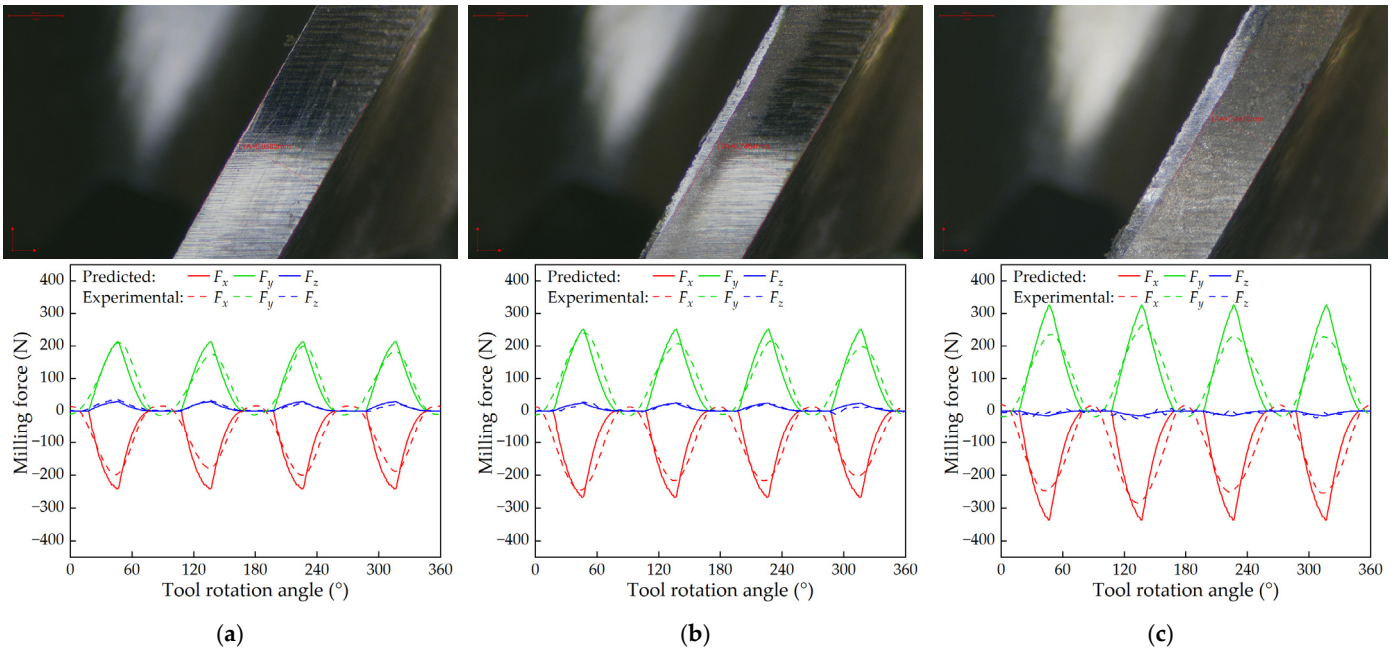


Figure 8. *Cont.*

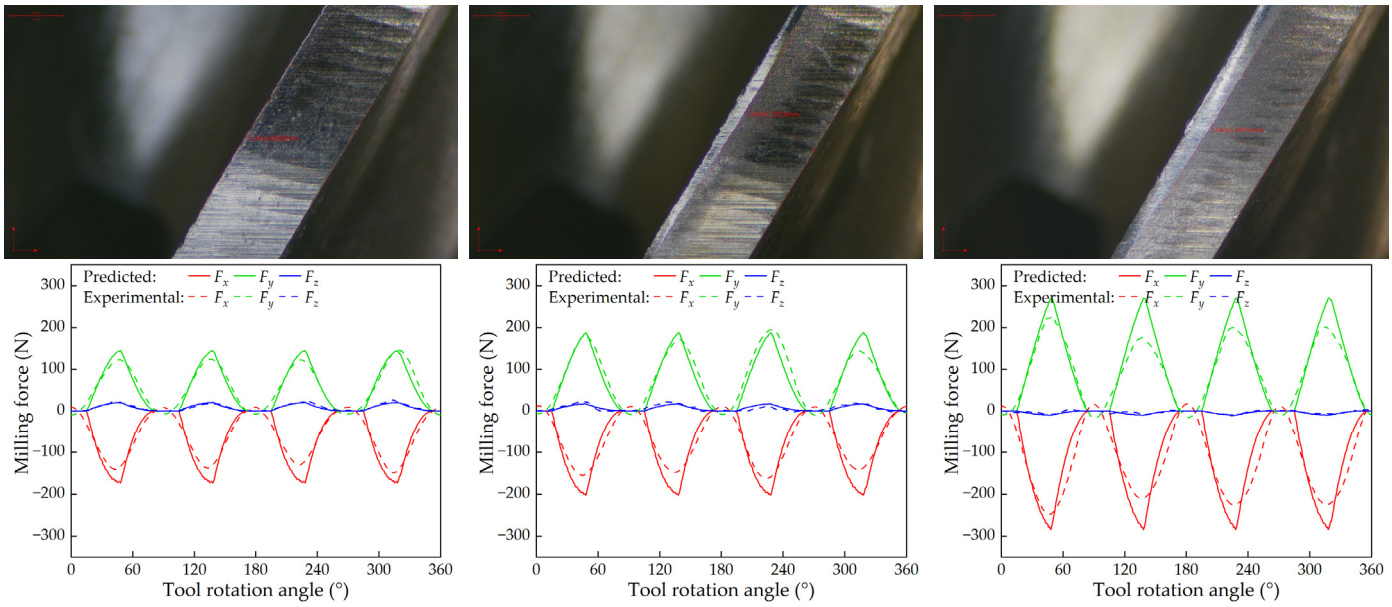


Figure 8. Tool flank-wear widths with corresponding milling forces: (**a**) Test.1; (**b**) Test.2; (**c**) Test.3; (**d**) Test.4; (**e**) Test.5; (**f**) Test.6.

Based on the results in the figure, it can be observed that the experimental milling-force curve aligns well with the predicted milling-force curve. A comparison of the average milling forces in the XYZ directions between the experimental and predicted models was conducted, and the corresponding errors were calculated. The results are shown in Figure 9.

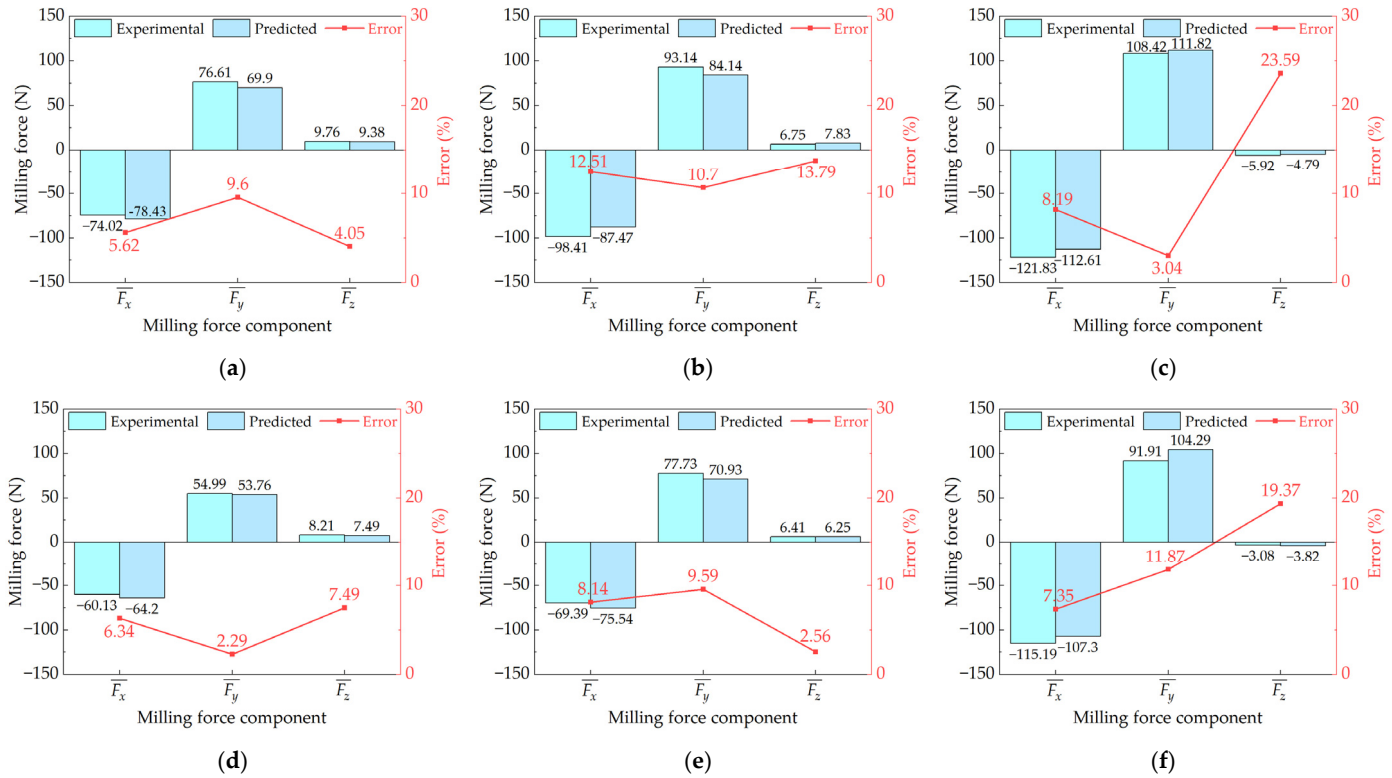


Figure 9. Comparison of experimental and predicted average milling forces: (**a**) Test.1; (**b**) Test.2; (**c**) Test.3; (**d**) Test.4; (**e**) Test.5; (**f**) Test.6.

From the results in the figure, it can be seen that the proposed model demonstrates strong predictive performance, with the comprehensive prediction errors of the average milling forces in the XYZ directions being 8.03%, 7.85%, and 11.81%, respectively. Therefore, the cutting-force prediction model for 304 stainless steel proposed in this paper, which accounts for tool wear, demonstrates reliable predictive accuracy.

4. Discussion

This study established a cutting-force model for milling 304 stainless steel, incorporating tool wear effects, based on side-milling experiments. Additionally, the study explored how milling forces vary with tool wear. This section discusses the research findings, existing limitations and potential industrial applications of the model.

1. To visually demonstrate the variation in milling forces with tool wear during the milling process, we used Equation (13) to calculate the average milling forces in the XYZ directions from the coefficient-identification experiment. The results are presented in Figure 10. From these results, it is clear that tool wear leads to an increase in the ploughing-force coefficient, which subsequently leads to a progressive rise in milling force. When the tool reaches its end of life (VB = 0.3), the increase in cutting force can exceed 100% compared to when the tool is sharp. This observation is consistent with the findings of most previous studies. Both the milling-force and ploughing-force coefficient increase at an accelerating rate as the tool wears. This behavior aligns with the findings in the study by Liu et al. [24]. Furthermore, the tangential contact-force coefficient is much larger than the radial contact-force coefficient—approximately twice as large. This pattern agrees with the findings of Chen et al. [34]. Their study focused on milling TC4; due to the differences in material properties, their study found that the tangential contact-force coefficient was approximately three-times larger than the radial contact-force coefficient. Therefore, the model proposed in this study is deemed reliable, although variations in milling force due to tool wear may differ across various tools and materials.
2. Discrepancies existed between the experimental and predicted values, especially when the tool flank wear was significant. These discrepancies are hypothesized to arise from several factors: On one hand, as tool wear progresses, especially when the tool flank-wear width (VB) becomes substantial, significant built-up-edge (BUE) formation and chip adhesion occur, as shown in Figure 11. These built-up edges and adhered chips replaced the original tool-edge geometry during the cutting process, significantly affecting the cutting force [30]. On the other hand, since neither the tool nor the workpiece is perfectly rigid, tool runout and workpiece deformation occur during the cutting process. The combined effects of these factors contribute to the discrepancies between the predicted and experimental cutting forces, especially when tool flank wear is significant.
3. Concerning the model's limitations, these primarily stem from two aspects:
    (a) Limitations in work condition universality due to the different material properties of various tools and workpiece materials, alongside their distinct contact characteristics. When the tool or material is changed, it is necessary to re-identify the coefficients in the milling-force model.
    (b) Limitations of simplifications and assumptions: In developing the model, certain factors (e.g., environmental temperature, cooling conditions, and the rigidity of the machine tool and clamping system) are often neglected or simplified to facilitate calculation and analysis. Consequently, the model may exhibit some errors. Therefore, when considering different machining

conditions, it is important to carefully evaluate which factors are necessary and which can be neglected to maintain the model's accuracy.

4. Regarding the potential industrial applications of the model, the following two scenarios merit discussion:
   (a) During the machining process: Tool wear leads to a significant increase in cutting force, subsequently affecting spindle torque, machine tool energy consumption, and vibration signals. Therefore, by monitoring these signal changes and combining them with the cutting-force model, tool wear can be estimated without stopping the machine, preventing the adverse effects of excessive tool wear on the machining process.
   (b) Before the machining process: Establishing a correlation between tool wear progression and machining parameters and applying the milling-force model to formulate and optimize the machining parameters will help to improve machining quality and efficiency.

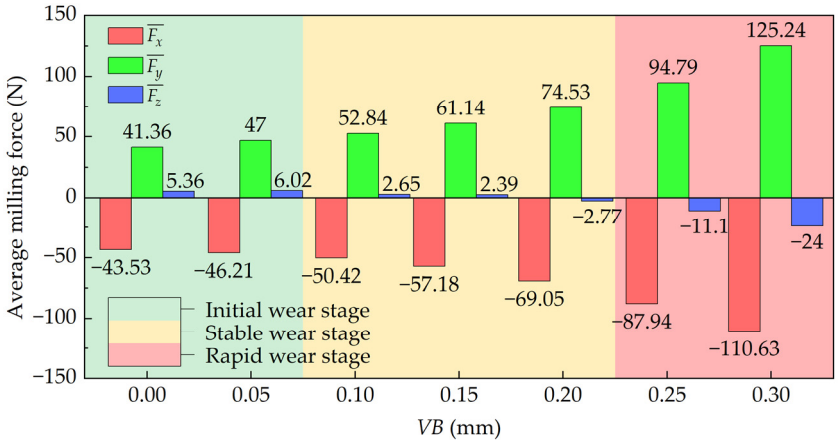
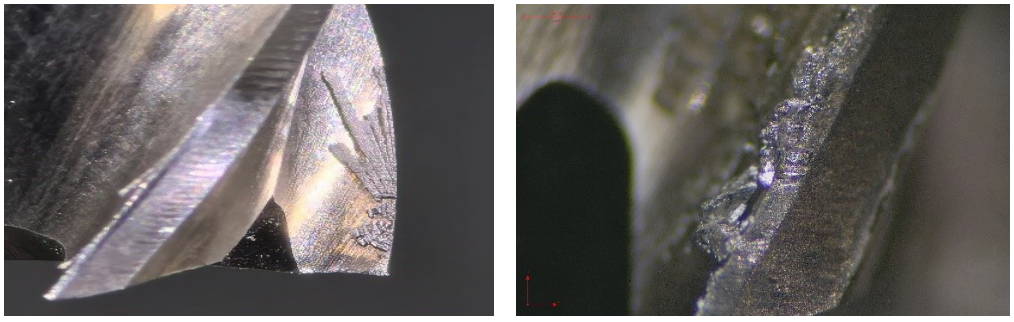


Figure 10. Variation of average milling force with tool flank-wear widths (*VB*).



(**a**) (**b**)

Figure 11. Chip adhesion and built-up edge (BUE) in the milling process: (**a**) Chip adhesion; (**b**) Built-up edge (BUE).

5. Conclusions

This paper develops a milling-force prediction model for 304 stainless steel that incorporates tool wear. Through conducting side-milling experiments on 304 stainless steel, the variation of milling force with tool wear was analyzed, and the accuracy of the proposed model was validated. The main conclusions are as follows:

1. Following the mechanistic modeling approach for cutting forces, the worn end mill was discretized into cutting-edge elements. The forces acting on these elements were studied. Considering the effect of tool wear on the actual radius of the end mill, the

tool–workpiece engagement relationship during the milling process was analyzed. A method for identifying the milling-force model coefficients under side-milling conditions has been developed. By integrating and summing, the instantaneous milling-force mechanistic model for the worn tool was formulated.

2. The side-milling experiments on 304 stainless steel revealed that with progressive wear on the flank face of the end mill, milling force increased at an accelerating rate. During the rapid-wear stage, the average milling force exerted by the worn end mill was more than twice that of the sharp tool. Therefore, developing a milling-force model that considers tool wear is crucial for the formulation and optimization of milling process parameters.
3. The established milling-force model can accurately predict the milling force of worn tools based on tool geometry and milling parameters. It can visually display cyclic fluctuations of milling force during tool engagement and disengagement under actual machining conditions.

The study proposes a milling-force prediction model for 304 stainless steel that incorporates tool wear considerations. The model demonstrates reliable predictive performance across various machining parameters and tool wear conditions and offers applicative value in relevant industrial settings.

Author Contributions: Conceptualization, Y.L. and C.W.; methodology, C.W.; software, K.W.; validation, K.W., K.Y. and P.H.; formal analysis, Y.L.; investigation, Y.X.; resources, F.G.; data curation, Y.X.; writing—original draft preparation, C.W.; writing—review and editing, C.W.; visualization, C.W.; supervision, Y.L.; project administration, Y.L.; funding acquisition, F.G. All authors have read and agreed to the published version of the manuscript.

Funding: This research was funded by the Shaanxi Province Modern Equipment Green Manufacturing Collaborative Innovation Center Project (No. 23JY054) and 'Leader Unveiling' projects for the industrialization of key core technologies in Shaanxi Province (No. 2205-610361-04-02-940891).

Data Availability Statement: Data are contained within the article.

Acknowledgments: Thanks to Xi'an University of Technology Shaanxi Provincial Key Laboratory of Manufacturing equipment to provide equipment support.

Conflicts of Interest: The authors declare no conflicts of interest.

References

1. Zhang, Z.; Zhang, H.; Liu, X.; Wang, T.; Huang, Q.; Liao, X. Effect of roll surface topography on microstructure and mechanical properties of 304 stainless steel ultra-thin strip. *J. Manuf. Process.* **2023**, *108*, 764–778. [CrossRef]
2. Korkut, I.; Kasap, M.; Ciftci, I.; Seker, U. Determination of optimum cutting parameters during machining of AISI 304 austenitic stainless steel. *Mater. Des.* **2004**, *25*, 303–305. [CrossRef]
3. Boillot, P.; Peultier, J. Use of stainless steels in the industry: Recent and future developments. *Procedia Eng.* **2014**, *83*, 309–321. [CrossRef]
4. Lo, K.H.; Shek, C.H.; Lai, J.K.L. Recent developments in stainless steels. *Mater. Sci. Eng. R Rep.* **2009**, *65*, 39–104. [CrossRef]
5. Kaladhar, M.; Subbaiah, K.V.; Rao, C.H.S. Machining of austenitic stainless steels—A review. *Int. J. Mach. Mach. Mater.* **2012**, *12*, 178–192. [CrossRef]
6. França, P.H.; Barbosa, L.M.; Fernandes, G.H.; Machado, Á.R.; Martins, P.S.; da Silva, M.B. Internally cooled tools: An eco-friendly approach to wear reduction in AISI 304 stainless steel machining. *Wear* **2024**, *554–555*, 205490. [CrossRef]
7. Wojciechowski, S.; Krajewska-Śpiewak, J.; Maruda, R.W.; Krolczyk, G.M.; Nieslony, P.; Wieczorowski, M.; Gawlik, J. Study on Ploughing Phenomena in Tool Flank Face–Workpiece Interface Including Tool Wear Effect during Ball-End Milling. *Tribol. Int.* **2023**, *181*, 108313. [CrossRef]
8. Ge, G.; Xiao, Y.; Lv, J.; Du, Z. A Non-Iterative Compensation Method for Machining Errors of Thin-Walled Parts Considering Coupling Effect of Tool-Workpiece Deformation. *Manuf. Lett.* **2024**, *41*, 287–295. [CrossRef]
9. Liu, C.; Huang, Z.; Huang, S.; He, Y.; Yang, Z.; Tuo, J. Surface roughness prediction in ball screw whirlwind milling considering elastic-plastic deformation caused by cutting force: Modelling and verification. *Measurement* **2023**, *220*, 113365. [CrossRef]

10. Shi, K.N.; Liu, N.; Liu, C.L.; Ren, J.X.; Yang, S.S.; Tan, W.C. Indirect approach for predicting cutting force coefficients and power consumption in milling process. *Adv. Manuf.* **2022**, *10*, 101–113. [CrossRef]
11. Bhushan, R.K. GA approach for optimization of parameters in machining Al alloy SiC particle composite for minimum cutting force. *J. Alloys Metall. Syst.* **2023**, *1*, 100002. [CrossRef]
12. Liu, T.; Song, J.; Zhang, K.; Liu, Q.; Chen, F. Tooth-wise monitoring of the asymmetrical tool wear in micro-milling based on the chip thickness reconstruction and cutting force signal. *Mech. Syst. Signal Process.* **2024**, *208*, 111004. [CrossRef]
13. Du, Y.; Song, Q.; Liu, Z. Prediction of Micro Milling Force and Surface Roughness Considering Size-Dependent Vibration of Micro-End Mill. *Int. J. Adv. Manuf. Technol.* **2022**, *119*, 5807–5820. [CrossRef]
14. Davoodi, B.; Tazehkandi, A.H. Experimental investigation and optimization of cutting parameters in dry and wet machining of aluminum alloy 5083 in order to remove cutting fluid. *J. Clean. Prod.* **2014**, *68*, 234–242. [CrossRef]
15. Merchant, M.E. Mechanics of the metal cutting process. I. Orthogonal cutting and a type 2 chip. *J. Appl. Phys.* **1945**, *16*, 267–275. [CrossRef]
16. Merchant, M.E. Mechanics of the metal cutting process. II. Plasticity conditions in orthogonal cutting. *J. Appl. Phys.* **1945**, *16*, 318–324. [CrossRef]
17. Altintas, Y. *Manufacturing Automation: Metal Cutting Mechanics, Machine Tool Vibrations, and CNC Design*; Cambridge University Press: Cambridge, UK, 2012.
18. Yang, D.; Zhang, Y.; Wang, R.; Wei, F.; Zeng, L.; Liu, M. Finite Element Modeling and Optimization Analysis of Cutting Force in Powder Metallurgy Green Compacts. *Processes* **2023**, *11*, 3186. [CrossRef]
19. Forootan, M.; Akbari, J.; Ghorbani, M. A real-time intelligent method to identify mechanistic cutting force coefficients in 3-axis ball-end milling process using stochastic gradient decent: The mechanistic network. *Int. J. Adv. Manuf. Technol.* **2023**, *129*, 2949–2968. [CrossRef]
20. Zhao, M.; Cai, Y.; Wang, N.; Song, Y.; Wang, H. The research of cutting force prediction for worn ball-end tool considering spring back. *Int. J. Adv. Manuf. Technol.* **2023**, *125*, 5619–5629. [CrossRef]
21. Wojciechowski, S.; Maruda, R.W.; Nieslony, P.; Krolczyk, G.M. Investigation on the edge forces in ball end milling of inclined surfaces. *Int. J. Mech. Sci.* **2016**, *119*, 360–369. [CrossRef]
22. Wang, W.; Tang, Y.; Guo, X.; Zhang, K.; Liu, T.; Wang, C. Modeling of cutting force in micro-milling considering asymmetric tool wear. *Int. J. Adv. Manuf. Technol.* **2024**, *133*, 1597–1608. [CrossRef]
23. Gao, S.; Duan, X.; Zhu, K.; Zhang, Y. Influence of tool flank wear considering tool edge radius on instantaneous uncut chip thickness and cutting force in micro-end milling. *Int. J. Adv. Manuf. Technol.* **2024**, *133*, 1639–1650. [CrossRef]
24. Liu, T.; Liu, Y.; Zhang, K. An improved cutting force model in micro-milling considering the comprehensive effect of tool runout, size effect, and tool wear. *Int. J. Adv. Manuf. Technol.* **2022**, *120*, 659–668. [CrossRef]
25. Wojciechowski, S.; Matuszak, M.; Powałka, B.; Madajewski, M.; Maruda, R.W.; Królczyk, G.M. Prediction of cutting forces during micro end milling considering chip thickness accumulation. *Int. J. Mach. Tools Manuf.* **2019**, *147*, 103466. [CrossRef]
26. Hou, Y.; Zhang, D.; Wu, B.; Luo, M. Milling force modeling of worn tool and tool flank wear recognition in end milling. *IEEE/ASME Trans. Mechatron.* **2014**, *20*, 1024–1035. [CrossRef]
27. Huang, Y.; Liang, S.Y. Modeling of cutting forces under hard turning conditions considering tool wear effect. *J. Manuf. Sci. Eng.* **2005**, *127*, 262–270. [CrossRef]
28. Chinchanikar, S.; Choudhury, S.K. Cutting force modeling considering tool wear effect during turning of hardened AISI 4340 alloy steel using multi-layer TiCN/Al_2O_3/TiN-coated carbide tools. *Int. J. Adv. Manuf. Technol.* **2016**, *83*, 1749–1762. [CrossRef]
29. Patel, V.D.; Gandhi, A.H. Modeling of cutting forces considering progressive flank wear in finish turning of hardened AISI D2 steel with CBN tool. *Int. J. Adv. Manuf. Technol.* **2019**, *104*, 503–516. [CrossRef]
30. Toubhans, B.; Fromentin, G.; Viprey, F.; Karaouni, H.; Dorlin, T. Machinability of Inconel 718 during turning: Cutting force model considering tool wear, influence on surface integrity. *J. Mater. Process. Technol.* **2020**, *285*, 116809. [CrossRef]
31. Teitenberg, T.M.; Bayoumi, A.E.; Yucesan, G. Tool wear modeling through an analytic mechanistic model of milling processes. *Wear* **1992**, *154*, 287–304. [CrossRef]
32. Martellotti, M.E. An analysis of the milling process. *Trans. Am. Soc. Mech. Eng.* **1941**, *63*, 677–695. [CrossRef]
33. *ISO 8688-2:1989*; Tool Life Testing in Milling—Part 2: End Milling. ISO: Geneve, Switzerland, 1989.
34. Chen, X.; Zhang, Z.; Wang, Q.; Zhang, D.; Luo, M. A new method for prediction of cutting force considering the influence of machine tool system and tool wear. *Int. J. Adv. Manuf. Technol.* **2022**, *120*, 1843–1852. [CrossRef]

Disclaimer/Publisher's Note: The statements, opinions and data contained in all publications are solely those of the individual author(s) and contributor(s) and not of MDPI and/or the editor(s). MDPI and/or the editor(s) disclaim responsibility for any injury to people or property resulting from any ideas, methods, instructions or products referred to in the content.